PCCP

Accepted Manuscript

ROYAL SOCIETY OF CHEMISTRY

www.rsc.org/pccp

Journal Name

RSCPublishing

COMMUNICATION

Entropy and Enthalpy Contributions to the Kinetics of Proton Coupled Electron Transfer to the $Mn_4O_4(O_2PPh_2)_6$ Cubane

Cite this: DOI: 10.1039/x0xx00000x

Received 09th December 2013,
Accepted 00th

DOI: 10.1039/x0xx00000x

www.rsc.org/

Thomas G. Carrell[b], Paul F. Smith[a], Joseph Dennes[b], and G. Charles Dismukes[a*]

The dependence of rate, entropy of activation, and ($^1H/^2H$) kinetic isotope effect for H-atom transfer from a series of p-substituted phenols to cubane $Mn_4O_4L_6$ (L=O_2PPh_2) (1) reveals the activation energy to form the transition state is proportional to the phenolic O-H bond dissociation energy. New implications for water oxidation and charge recombination in photosystem II are described.

The interdependence of proton and electron transfer kinetics, termed proton-coupled electron transfer (PCET), is common in chemical and biological redox reactions. This coupling is manifested in kinetics being controlled by the free energy difference and nuclear reorganization barrier between redox reaction partners[1]. A prominent example of PCET occurs in natural photosynthesis, in which water is oxidized by a $CaMn_4O_5$ "heterocubane" cluster (water oxidation complex, WOC) located in photosystem II (PSII). The cluster is capable of breaking four water O-H bonds (119 kcal/mol) via successive or concerted PCET reactions, many of which are believed to involve separate sites for the proton and electron. The $Mn_4O_4(O_2PPh_2)_6$ cubane (**1**) (Scheme 1A) is a related model compound that can dehydrogenate C-H, N-H, and O-H bonds and thus is useful for understanding successive PCET reactions[2,3]. Mechanistic studies have shown initial H-atom abstraction to form $Mn_4O_3(OH)(O_2PPh_2)_6$ (**1H**), which was isolated and characterized[4,5]. Depending upon reductant, three additional H equivalents can be removed to form the "butterfly" $Mn_4O_2(O_2PPh_2)_6$ (**2**) and release two water molecules (Scheme 1B). The O-H bond dissociation energy (BDE) of **1H** was previously estimated from such studies.

Herein, we have extended this work to examine the reaction kinetics and H/D kinetic isotope effect (KIE) between **1** and a series of para-substituted phenols of known O-H BDEs. The reaction between **1** and phenol has been previously reported and is summarized in Scheme 1[5]. The phenoxyl radical product R-PhO● is highly reactive and, depending on R, can further react to give a variety of radical coupling products. For phenol (R=H), this product is commonly biphenoquinone, but for p-substituted phenols, products may not easily be identified[5,6]. In our case, reaction of **1** with excess 4-methylphenol resulted in uniform spectral bleaching (Figure 1). Spectral bleaching is fully consistent with proton-coupled reduction of **1,** as previously observed by electrochemical methods[7]. The rate of bleaching is first order in [**1**] (Figure 1, inset), and can be fit to integrated first-order kinetics to determine the pseudo-first order constant (see SI for details). A plot of pseudo-first order rate constants vs. concentration of 4-methylphenol gives clean second order kinetics over ten-fold concentration range, R^2= 0.94 (Figure S1), and a second order rate constant of 4.80 $(M*s)^{-1}$. Eyring analysis (Figure S2) of the temperature dependence of the rate constant (10-30 ºC) gives the activation enthalpy and entropy of reaction ($\Delta H^{\ddagger}$ =2.8 kcal/mol and $\Delta S^{\ddagger}$ =-46 cal/mol*K, respectively). Thus, it follows that the activation energy at 298 K is $\Delta G^{\ddagger}$ = 16.5 kcal/mol.

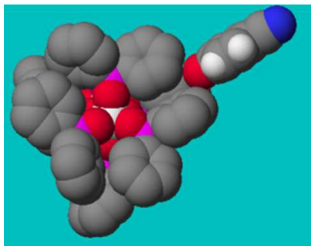

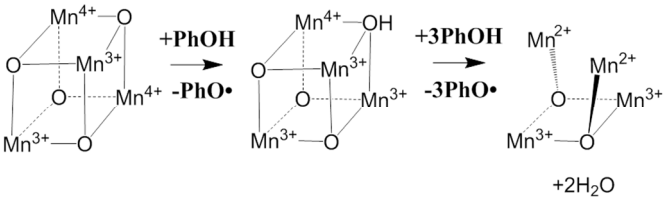

Scheme 1: (A, top) Postulated docking configuration of 4-methylphenol to the atomic structure of **1** taken from single crystal Xray diffraction. Image along one of the four body diagonals depicting Mn on top. Red = O, Purple = P, Silver = Mn, Gray = Phenyl ring, Blue = para-substituent. (**B, bottom**) Reactions of the $Mn_4O_4^{6+}$ cubane core with hydrogen atom donors.

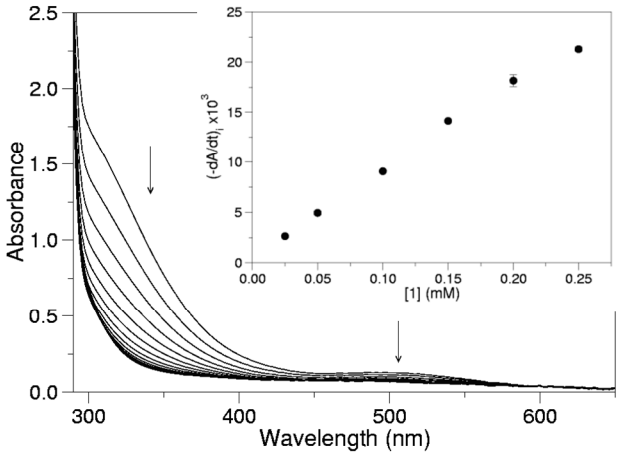

Figure 1: Spectral changes observed during the reaction of *p*-Me-phenol with **1** at 25.0ºC. Conditions: [**1**] = 0.10 mM in CH_2Cl_2; [*p*-Me-phenol] = 3.0 mM; spectra were collected in 20 second intervals. Inset: Initial rate $(-dA/dt)_i$ (at 342 nm) is a linear function of the concentration of **1** (R^2=0.99).

Scheme 2: Thermochemical cycle for **1.**

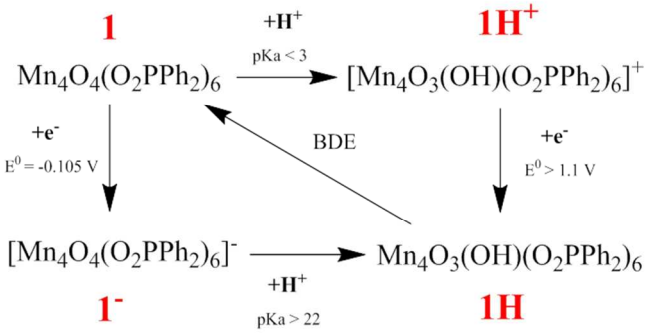

Table 1. Rate constants and linear free energy parameters for the reaction of **1** + 4-R-phenol.

R	$k, M^{-1}s^{-1}$	k_H/k_D	$\Delta G^{\ddagger a}$	$\Delta G^{o}_{CT}{}^{b}$	$\Delta G^{o}_{PT}{}^{b}$	$\Delta G^{o}_{ET}{}^{b}$	*O-H BDE*[c]
Me	4.80	2.0	16.5	≤4.7	≥21.8	45.4	88.7
H	0.71	n/a	18	≤5.9	≥20.5	47.9	89.8
Ph	27.5	n/a	15.5	≤3.6	≥19.3	42.4	87.6
tBu	6.53	n/a	16.3	≤4.8	≥21.9	45.6	88.7
Br	2.44	n/a	16.9	≤6.8	≥18.3	49.8	90.7
CN	0.004	2.1	20	≤10.3	≥13.9	58.8	94.2

a. Experimentally measured, kcal/mol.
b. Calculated from thermochemical cycle, kcal/mol.
c. Phenol O-H bond dissociation energy, ref. [8]

Extending this workup to other para-substituted phenols (R= Ph, H, CN, tBu, Br), we obtain second order rate constants that cover four orders of magnitude and associated activation energies ($\Delta G^{\ddagger}$) within the range 15.5-20 kcal/mol (Table 1). Kinetic isotope effects (k_H/k_D) were measured at 298 K for monodeuterated p-Me and p-CN phenols, obtained by prior exchange in CH_3OD yielding values of 2.0±0.2 and 2.1 ±0.3, respectively. This implies KIE is essentially independent of BDE (Table 1).

Quantitative analysis shows that proton and electron transfer occur in a concerted mechanism, not successive stepwise pathways, as detailed next. The thermochemical cycle given in Scheme 2 depicts the contributions from pKa values[5] and reduction potentials[7] that convert the cubane **1** to its protonated (**1H**$^+$), reduced (**1**$^-$), and hydrogenated (**1H**) products. The reduction potential for **1H**$^+$/**1H** is at least equal that of **1**$^+$/**1,** because **1H**$^+$ quantitatively oxidizes **1** to **1**$^+$ as described previously[9]. The parameters from this cycle are converted to Gibbs energy using eqns (1-3)[10]:

$$\Delta G^{o}_{PT} = 1.37[pK_a(\text{Ph-OH}) - pK_a(\mathbf{1H^+})] \quad (1)$$

$$\Delta G^{o}_{ET} = 23.06[E^{o}(\text{Ph-OH}\bullet/\text{Ph-OH}) - E^{0}(\mathbf{1/1^-})] \quad (2)$$

$$\Delta G^{0}_{PCET} = 23.06[E^{o}(\text{Ph-OH}\bullet/\text{Ph-OH}) - E^{o}(\mathbf{1/1^-})] + 1.37[pKa(\text{Ph-OH}\bullet) - pKa(\mathbf{1H})] \quad (3)$$

The calculated thermodynamic driving force for the first proton transfer from the phenol to **1** (ΔG^{o}_{PT}) is proportional to the difference between the pK_a values of the phenol (ca. 19 for 4-methylphenol)[8] and **1**, which can be protonated only by strong acids. Thus, the first proton transfer from 4-methylphenol to **1** is uphill by at least 1.37*(16) = 21.8 kcal/mol. This thermodynamic barrier is larger than the kinetic activation energy measured experimentally. Likewise, the necessary driving force for initial electron transfer (ΔG^{o}_{ET}) is proportional to the difference in the one-electron reduction potentials. The first electron transfer step from 4-methylphenol ($E_{1/2}$ = 1.865 V vs. SHE)[8] to **1** (-0.105 V vs. SHE) is uphill by 45.4 kcal/mol, which is again larger than the experimental activation energy. For all phenols studied, the measured $\Delta G^{\ddagger}$ is lower than the values expected if either the proton or electron were transferred individually (Table 1), with one exception (proton transfer from 4-CN-phenol, ΔG^{o}_{PT}). This data strongly infers that stepwise PCET does not occur in this system.

For concerted transfer (ΔG^{o}_{CT}), the change in free energy is calculated as the sum of two processes- first, electron transfer from 4-methylphenol to **1**, and second, proton transfer from the resulting radical cation to the reduced cube (eqn 3). The latter process has a very negative Gibbs energy, because the 4-methylphenol radical cation (Ph-OH●, pKa = -7.1)[8] transfers a proton to the strongly basic **1**$^-$ at least 29 pK units. As a result, ΔG^{o}_{CT} is much lower than the calculated ΔG^{o}_{PT} and ΔG^{o}_{ET} values; CT from 4-methylphenol to **1** is calculated as ≤ 45.4-1.37*(29) = 4.7 kcal/mol. For all phenols, we find $\Delta G^{o}_{CT} <\leq \Delta G^{\ddagger}$. Thus, CT is not only the thermodynamically favored pathway; it is also the *only* pathway with a calculated driving force lower than the measured activation energy.

This approach allows an estimation of the O-H BDE of **1H** via eqn (4)[11]. From the reaction with 4-methylphenol:

$$4.7 \leq \Delta G^{o}_{rxn} = (BDE_{1H} - BDE_{phenol}) - T(\Delta S^{o})_{rxn} \quad (4)$$

$$BDE_{1H} = BDE_{phenol} + \Delta G^{o}_{rxn} + T\Delta S^{o}_{rxn} \leq 88.7 + 4.7 + T\Delta S^{o}_{rxn}$$

Where the subscript rxn denotes the measured reaction:

1 + PhOH → (**1H**●OPh) → **1H** + ●OPh

Ignoring the entropy term, this gives $BDE_{1H} \leq 93.4$ kcal/mol. The highest upper bound obtained in this way is ≤ 98.9 kcal/mol (R = CN). The actual BDE is likely lower due to the negative TΔS term

(see below). We note that a lower bound can be calculated by adapting the common thermodynamic cycle[5,8,12–14]:

$$BDE = 23.06E_{1/2} + 1.37\ pK_a + 56\ (kcal/mol) \quad (5)$$

Using $E_{1/2}$(**1**/**1**$^-$) and pKa (**1H**/**1**$^-$) in eqn(5) gives a lower bound BDE ≥ 84 kcal/mol. Combining these results, the homolytic BDE lies in the range of 84-98.9 kcal/mol. The range for heterolytic BDE (**1H** → **1**$^+$ + H$^-$) is likewise determined by adding $23.06(E_{1/2}(\mathbf{1}^+/\mathbf{1}))$[5], yielding 109.4-124.3 kcal/mol. This range compares to the heterolytic BDE of 122 kcal/mol for $[L_2Mn(\mu\text{-}O)(\mu\text{-}OH)MnL_2]^{3+}$ (L=1,10-phenanthroline)[15,16], which has a higher average Mn oxidation state (3.5 vs. 3.25 in **1H**).

For PCET reactions from a class of similar substrates, Bell-Evans-Polanyi kinetics predict linear correlation between activation energy (proportional to ln(k)) and homolytic bond dissociation energy of the PhO-H bond[10,13,17]. As Figure 2 illustrates, this correlation (R^2 = 0.97) is indeed present for all the phenols studied, including the N-H bond of phenothiazine (pzH). This correlation covers seven orders of magnitude and strongly implies that H-atom transfer to **1** proceeds by a similar mechanism from all these H-donors. As expected, linear correlations also exist with the donor reduction potential (R^2 = 0.94) and pK$_a$ (R^2 = 0.80), although neither fits as well as the BDE (Figure S3).

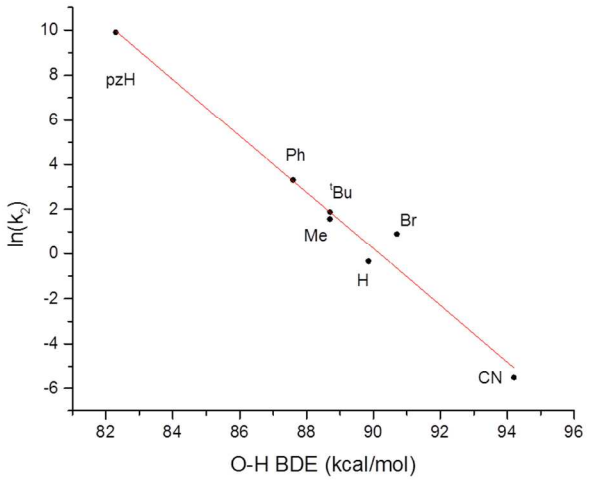

Figure 2: Dependence of ln(k_2) on the homolytic bond dissociation energy.

At 298 K, the entropy term is by far the dominant contributor to the activation energy ($-T\Delta S^{\ddagger}$ = 13.7 kcal/mol vs. $\Delta H^{\ddagger}$ = 2.8 kcal/mol for 4-MePhenol), indicating that the transition state is dominated by an increase in order rather than PhO-H bond breaking. This result is rationalized because H-atom transfer occurs via an inner-sphere mechanism; for the phenol to make van der Waals contact with a corner oxo, reordering of the phenyl rings of three phosphinate ligands is required to allow phenol access (Scheme 1A), as previously observed for bulky H donors[5]. Additionally, the presence of a small KIE (k_H/k_D ~ 2.0) is consistent with this result as it implies little O-H bond cleavage in the transition state[18]. Our data suggest an ordered transition state involving significant reorganization of the Ph ligands of **1** to allow close contact between the phenol and corner oxo of **1** which allows H-atom transfer (Scheme 1A illustrates the reactants approaching). This transition state has lower entropy than the separate reactants, likely a result of the additional steric congestion around the $[Mn_4O_4]^{6+}$ core of **1** created by the 12 phenyl rings from six facially bridging $Ph_2PO_2^-$ ligands. The X-ray structure of **1** reveals these rings pack to form a hydrophobic propeller-shaped cavity from three adjacent phenyl rings[19]. These phenyls must move apart to allow the phenol to reach the corner oxygen atoms of **1**.

We note that the linear dependence in Figure 2 of ln(k_2) vs O-H BDE is not in accord with simple Marcus theory which scales as $\log(k_{ET}) \sim (\Delta G)^2$ for adiabatic reactions governed by parabolic potential energy surfaces[10,20]. We find this outcome to be self-consistent with the kinetic model predicting a dominant and relatively constant entropy term contributing to the reduction of **1** by phenols.

The homolytic μ-(O-H) BDE determined herein for **1H** is stronger than for all $[Mn_2O(OH)]^{3+/3+}$ complexes in the literature that have been measured to our knowledge (76-84 kcal/mole, S. I., Table S1)[13,21,22]. This difference originates from the weaker Mn-O bonding in **1** (longer Mn-O bond lengths, ΔR~ 0.2 Å) vs the rhombohedral $[Mn_2O_2]^{4+}$ core complexes. This core expansion indicates greater 4s orbital and reduced 3d orbital character from Mn in the HOMO. Consequences for **1** include greater valence electron delocalization (reduced mixed valency Mn^{III}:Mn^{IV}) , higher symmetry (tetrahedral) core, and weaker electrochemical reduction potential (**1**/**1**$^-$) relative to comparable $[Mn_2O_2]^{4+}$ core complexes. The reduction of **1** involves loss of delocalization of the two highest valence electrons in the HOMO of the symmetrical core. Nature's choice of calcium in the $CaMn_4O_5$ core of Photosystem II may serve to suppress valence delocalization, in light of a recent report indicating that a $CaMn_3O_4$ heterocubane is more easily oxidized (has lower reduction potential) than the Mn_4O_4 core in the same ligand set[23].

Conclusion

The mechanism responsible for controlling the rate of hydrogenation of the cubane **1** by a range of phenol derivatives has been examined by kinetics and KIE covering seven orders of magnitude in rate constant. The free energy barrier controlling the rate of this bimolecular reaction is composed of two terms: mainly an entropy penalty attributed to formation of the reactive complex upon insertion of the phenol between the geared rings of the diphenylphosphinate ligands (Scheme 1), and, by a smaller enthalpy term after forming the reactive complex that scales linearly with the O-H bond dissociation energy. The small BDE-independent KIE observed is consistent with this picture of the reaction coordinate. A small KIE is observed also for the various S-state transitions in PSII-WOC[24], which are likewise viewed as PCET processes in the early S-state transitions[4,25]. The O-H bond of water (119 kcal/mol) is substantially lowered by complexation as a bridging hydroxo between manganese atoms, considerably more so for di-μ-OH than for tri-μ-OH sites. These results show that the stronger tri-μ-OH bond in **1H** conserves a larger fraction of the available free energy of the phenol O-H bond, but at the expense of a much slower forward rate. As a result the reverse PCET step becomes important and this has important implications for the functioning of the PSII-WOC in photosynthesis. Indeed, a number of papers have reported reverse electron transfer (PCET) between the WOC and $Y_Z^{\bullet}$ from low temperature trapped S_i states, using infrared light absorbed by the Mn cluster to overcome activation barriers[26]. Hence, the state energy difference between these states is relatively small.

Scheme 3: The environment surrounding the tyrosine oxidant in

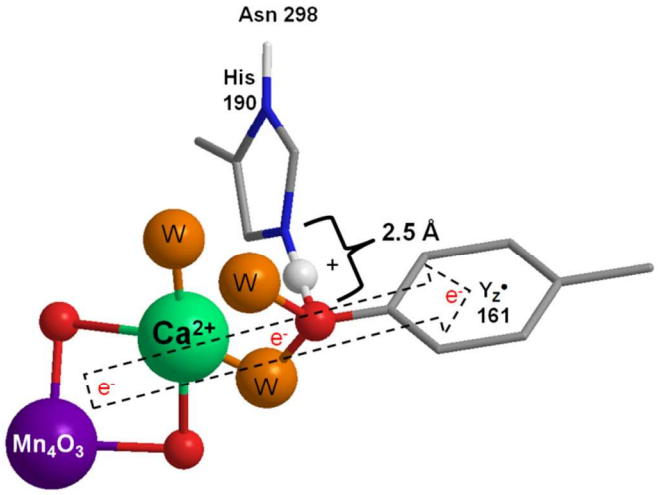

Scheme 3 shows the environment of D_1-tyrosine161 (Y_Z-OH) in photosystem II, derived from the 1.9Å X-ray structure[27]. With an O-H BDE of 86.5 kcal/mol[28] (E^o = 1.21 V)[29], $Y_Z^\bullet$ can oxidize the $CaMn_4O_5$ (WOC) when H^+ evolution is permitted. This reaction is blocked (reversed) if protons derived from water oxidation accumulate within the WOC[30]. The present work indicates that the rate of the analogous PCET reaction between **1** and PhOH in solution is controlled both entropically by attainment of a close encounter complex, **1H●**OPh, and enthalpically by the relative strengths of their O-H bonds. Oxygenic photosynthesis relies upon both strategies for creating selective oxidation of the WOC by specific associations of Y_Z-OH with its surroundings. As shown in Scheme 3, electrostatic activation of Y_Z-OH/$Y_Z^\bullet(H^+)$ is achieved by prevention of H^+ release via strong H-bonding to D_1His190 (denoted here by (H^+)), and by electrostatic polarization from coordinated Ca^{2+}. These charges help create both the high oxidation potential of Y_Z-OH/$Y_Z^\bullet(H^+)$ and provide a positive electrical potential gradient from $Y_Z^\bullet(H^+)(Ca^{2+})$ to the Mn_4O_5 subcluster that facilitates forward electron transfer (S-state transitions):

$$S_iY_Z^\bullet(H^+) \leftrightarrow S_{i+1}(+)Y_ZOH \rightarrow S_{i+1}Y_ZOH + H^+$$

Importantly, the reverse reaction is slowed greatly by proton transfer from (H^+)His190 that traps the electron, yielding neutral Y_ZOH. This PCET function of $Y_Z^\bullet(H^+)$His190 is often overlooked but is a critical function, as it keeps the site of oxidation within the Mn_4O_5 subcluster, $(S_{i+1})(+)$, rather than on $Y_Z^\bullet(H^+)$. This trapping slows the charge recombination reactions with the terminal acceptors (plastosemiquinones) Q_A^- and Q_B^- located in PSII[26]. The $Y_Z^\bullet(H^+)$His190 molecular diad is analogous to a pn-diode, designed foremost to prevent reverse electron flow and keep the accumulated holes in the Mn_4O_5 subcluster where O_2 evolution can be catalyzed.

This work was supported by the National Science Foundation (CLP-CHE1213772), an NSF IGERT fellowship (P.F.S.), and an NSF REU fellowship (J.D.).

Notes and references

[a]Department of Chemistry and Chemical Biology, Rutgers University, Piscataway NJ 08854.

[b]Department of Chemistry, Princeton University, Princeton NJ 08540

*To whom correspondence should be addressed. Email: dismukes@rci.rutgers.edu

Electronic Supplementary Information (ESI) available: Materials and methods, procedures for kinetic measurements and data analysis, and Figures S1-S3. See DOI: 10.1039/c000000x/

1. S. Hammes-Schiffer, *Energy Environ. Sci.*, 2012, **5**, 7696–7703.
2. W. F. Ruettinger and G. C. Dismukes, *Inorg. Chem.*, 2000, **39**, 1021–1027.
3. T. G. Carrell, S. Cohen, and G. C. Dismukes, *J. Mol. Catal. A Chem.*, 2002, **187**, 3–15.
4. M. Maneiro, W. F. Ruettinger, E. Bourles, G. L. McLendon, and G. C. Dismukes, *Proc. Natl. Acad. Sci. U. S. A.*, 2003, **100**, 3707–3712.
5. T. G. Carrell, E. Bourles, M. Lin, and G. C. Dismukes, *Inorg. Chem.*, 2003, **42**, 2849–2858.
6. A. Al-Ajlouni, A. Bakac, and J. H. Espenson, *Inorg. Chem.*, 1993, **32**, 5792–5796.
7. R. Brimblecombe, A. M. Bond, G. C. Dismukes, G. F. Swiegers, and L. Spiccia, *Phys. Chem. Chem. Phys.*, 2009, **11**, 6441–6449.
8. We adopt the BDE's as determined from the thermodynamic cycle in: F. G. Bordwell and J. Cheng, *J. Am. Chem. Soc.*, 1991, **113**, 1736–1743. These solution-phase values match experimental gas-phase literature to ±3 kcal/mol, see Bordwell, Cheng and Harrelson, J. Am. Chem. Soc, 1988, 110, 1229-1231
9. W. F. Ruettinger, D. M. Ho, and G. C. Dismukes, *Inorg. Chem.*, 1999, **38**, 1036–1037.
10. J. M. Mayer, *Annu. Rev. Phys. Chem.*, 2004, **55**, 363–390.
11. G. Yin, A. M. Danby, D. Kitko, J. D. Carter, W. M. Scheper, and D. H. Busch, *J. Am. Chem. Soc.*, 2008, **130**, 16245–16253.
12. M. J. Baldwin and V. L. Pecoraro, *J. Am. Chem. Soc.*, 1996, **118**, 11325–11326.
13. K. Wang and J. M. Mayer, *J. Am. Chem. Soc.*, 1997, **119**, 1470–1471.
14. V. D. Parker, K. L. Handoo, F. Roness, and M. Tilset, *J. Am. Chem. Soc.*, 1991, **113**, 7493–7498.
15. M. A. Lockwood, K. Wang, and J. M. Mayer, *J. Am. Chem. Soc.*, 1999, **121**, 11894–11895.
16. A. S. Larsen, K. Wang, M. A. Lockwood, G. L. Rice, T.-J. Won, S. Lovell, M. Sadílek, F. Turec□ek, and J. M. Mayer, *J. Am. Chem. Soc.*, 2002, **124**, 10112–10123.
17. J. P. Roth and J. M. Mayer, *Inorg. Chem.*, 1999, **38**, 2760–2761.
18. A. Hazra, A. V Soudackov, and S. Hammes-Schiffer, *J. Phys. Chem. Lett.*, 2010, **2**, 36–40.
19. W. F. Ruettinger, C. Campana, and G. C. Dismukes, *J. Am. Chem. Soc.*, 1997, **119**, 6670–6671.
20. R. A. Marcus and N. Sutin, *Biochim. Biophys. Acta - Rev. Bioenerg.*, 1985, **811**, 265–322.
21. M. T. Caudle and V. L. Pecoraro, *J. Am. Chem. Soc.*, 1997, **119**, 3415–3416.
22. H. H. Thorp, J. E. Sarneski, G. W. Brudvig, and R. H. Crabtree, *J. Am. Chem. Soc.*, 1989, **111**, 9249–9250.
23. J. S. Kanady, E. Y. Tsiu, M. W. Day, and T. Agapie, *Science*, 2011, **333,** 733-736.
24. M. Karge, K.-D. Irrgang, and G. Renger, *Biochemistry*, 1997, **36**, 8904–8913.
25. H. Kühne and G. W. Brudvig, *J. Phys. Chem. B*, 2002, **106**, 8189–8196.
26. N. Ioannidis, G. Zahariou, and V. Petrouleas, *Biochemistry*, 2008, **47**, 6292–6300.
27. Y. Umena, K. Kawakami, J.-R. Shen, and N. Kamiya, *Nature*, 2011, **473**, 55–60.
28. C. Tommos, C. W. Hoganson, M. Di Valentin, N. Lydakis-Simantiris, P. Dorlet, K. Westphal, H.-A. Chu, J. McCracken, and G. T. Babcock, *Curr. Opin. Chem. Biol.*, 1998, **2**, 244–252.
29. M. Grabolle and H. Dau, *Biochim. Biophys. Acta - Bioenerg.*, 2005, **1708**, 209–218.
30. D. J. Vinyard, G. M. Ananyev, and G. C. Dismukes, *Annu. Rev. Biochem.*, 2013, **82**, 577–606.

TOC Graphic and Textual Abstract

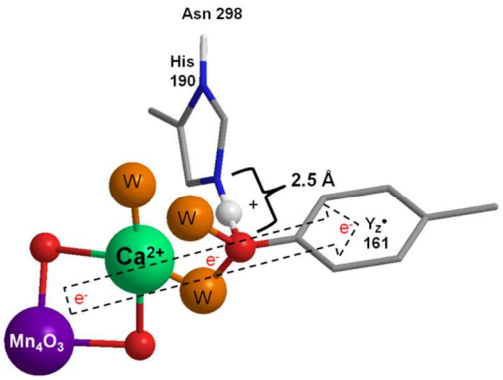

The reaction of a manganese-oxo cubane with hydrogen atom donors effectively models water oxidation and charge transfer in natural photosynthesis.